Chapter 7

Characterization of Nanocomposites Structure

Kristiina Oksman[1] and Robert J Moon[2,3]
[1] *Composite Center Sweden, Division of Materials Science, Luleå University of Technology, Luleå, Sweden*
2 USDA-Forest Service, Forest Products Laboratory, Madison, WI, USA
[3] *School of Materials Engineering and Birck Nanotechmology Center, Purdue University, West Lafayette, IN, USA*

This chapter summarizes several techniques that have been used in the characterization of cellulose nanocomposites, in particular cellulose nanomaterials (CNs) dispersion, distribution, and orientation within polymer matrixes. The microscopy techniques described are optical microscopy, scanning electron microscopy, transmission electron microscopy, and atomic force microscopy. Also, the use of X ray diffraction for quantification of CN orientation is discussed. The characterization of bionanocomposites is challenging because these materials are soft, moisture sensitive, non-conductive, and usually both the matrix phase and the reinforcement phase primarily consist of low atomic number elements (making differentiation difficult). Different sample preparation techniques for CN composite materials are also discussed.

7.1. Introduction

To take advantage of nanoscale features and create nanocomposites based on plant biomass, reliable characterization measurements are needed to resolve nanosized-scale features so that the "nanoeffect" can be elucidated. Although nanoscale measurement methods have expanded in recent years, not all these techniques are useful for soft, hydrophilic, non-conducting biomass specimens. This chapter summarizes several methods that have been shown to be particularly useful in nanoscale characterization of cellulose nanocomposite surfaces, cellulose nanomaterial (CN) distribution, dispersion, and their orientation within the polymer matrix.

The structure of polymer nanocomposites is traditionally characterized by a combination of transmission electron microscope (TEM) and wide-angle X-ray diffraction (WAXD).[1] This combination is, however, convenient only for layered silicate-based nanocomposites because of the ordered stacking of the silicate layers. For cellulose, only the 3D arrangement of the cellulose chains in the crystallites is detectable in WAXD and no peaks corresponding to the stacking of the crystallites can be observed in the nanocomposites.

Table 7.1. Resolution of the different microscopy techniques.

Technique	OM	SEM	FESEM	TEM	AFM
Resolution	0.2–1.3µm	5 nm	1 nm	0.2 nm	1 nm (x,y) 0.1 nm(z)

For observation of the nanostructure, different microscopy techniques can be utilized. In general, bionanocomposites are non-conductive, soft, and moisture-sensitive materials and therefore the sample preparation and microscopic characterization are challenging. For example, the use of electron microscopes will, in particular, require special attention to electron dose, contrast, and methods to assess the bulk structure without affecting the nanocomposites morphology.

Optical microscopy (OM), scanning electron microscopy (SEM), TEM, and atomic force microscopy (AFM) have been applied to study the structure, size, and morphology of cellulose nanocrystals (CNCs) and cellulose nanofibrils (CNFs).[2-6] Typically, SEM has been used most for the characterization of nanocomposites structure[7-14] even though the resolution is limited, as compared to AFM or TEM, and detailed information of the CN distribution within the polymer matrix is difficult to obtain. There are, however, SEM microscopes and field emission gun scanning electron microscopes (FESEM) with higher resolution comparable with TEM, but operate at very low voltages, making it possible to observe organic materials without conductive coating. AFM[14-17] and TEM[12,13,18-20] have also been utilized in studies on nanocomposites structure, especially the distribution and dispersion of cellulose or chitin nanomaterials. Table 7.1 shows the maximum resolution of the different microscopy techniques.[21,22]

The following sections describe the common sample preparation for microscopy studies of nanocomposites and some examples of micro- and nanostructures of the composite materials are shown which are viewed using different microscopy techniques.

7.2. Sample preparation

The most commonly used way to study the microstructure of nanocomposites is to examine fractured surfaces. The problem with this is that polymer nanocomposites are non-conducting and when imaged using SEM, the surfaces are usually coated with a thin layer (<10 nm) of conducting material (typically gold or platinum), otherwise the high intensive electron beam, that is focussed on the sample surface, can damage the surface. However, this coating will cover the finer details on the surface and may also create other artifacts (cracks, altered surface roughness, etc.). Figure 7.1 shows a platinum-coated cellulose nanocomposite where the coating has cracked and the underlying structure is visible.

Another sample preparation method for studies of cellulose nanocomposites structure is ultramicrotoming. This is a method where ultrathin (<100 nm) samples are produced and these are usually used for TEM imaging or when very smooth

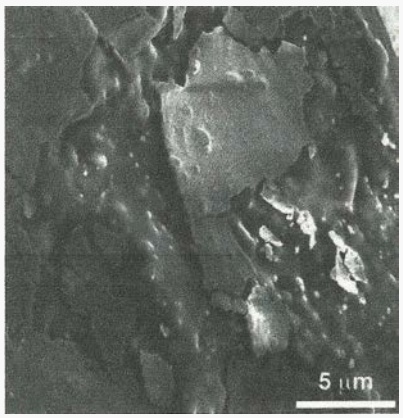

Fig. 7.1. FESEM image of platinum-coated nanocomposites of CNCs and polylactic acid (PLA), the coating has cracked and the underlying structure is visible.

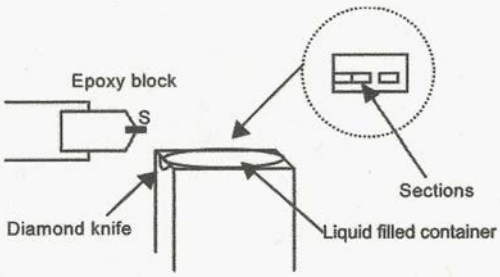

Fig. 7.2. Ultramicrotoming of the thin slices. S is the sample embedded in epoxy and sliced using a diamond knife and collected from a liquid-filled container. (Figure is based on Ref. 21.)

surfaces are needed for AFM studies. This is a common sample preparation method for polymeric materials. Ultramicrotomed samples will give information of actual "bulk" structure of the composite material. The sample is prepared using the following three steps: (i) the specimen is first embedded in a thermosetting resin and cured, (ii) then it is trimmed and sliced using microtome, and finally (iii) the thin slices can be stained if needed.

To obtain good sectioning, it is important that the hardness of the embed—polymer matches the hardness of the sample. Epoxies are typically used as the embedding polymer because they are stable in the electron beam. The schematic of the ultramicrotoming is shown in Fig. 7.2.

After the microtoming procedure, the slices are mounted on grids. The thickness of the slices is usually less than 100 nm, and in TEM imaging allows sufficient electron transmission through the sample to obtain a signal for imaging. It is important to slice the samples to an even thickness to avoid artifacts such as mass-thickness contrast.

Polymers with glass transition temperature below room temperature can be too soft for sectioning at room temperature. In this case, ultramicrotoming is

performed at low temperature using liquid nitrogen. The method is called cryo-ultramicrotoming. The advantages of cryo-technique are that embedding is not needed and soft polymers can be sectioned. Disadvangages are that this technique is more time consuming, it is also difficult to collect the sectioned samples, and frost could build-up.[23]

Freeze-etching method is an alternative to cryo-ultramicrotomy and can be used for water-soluble or soft polymers and this method is especially useful for beam-sensitive materials. The advantage of the freeze-etching technique is that there is no need for chemical fixation or staining of the sample. The freeze-etching method involves the following steps:

- rapid freesing,
- freeze fracturing or etching,
- shadowing, and
- replication and replica cleaning by dissolving the specimen.[24]

For the rapid freezing step, the polymer sample is mounted on a support and rapidly immersed in liquid nitrogen and placed in a cooled chamber and fractured. The freshly cleaved surface is either etched or fractured and shadowed with carbon or metallic deposition and a replication is made with a thin layer of carbon. The replica is taken off the sample, washed, and gathered onto TEM grids. The replica is an inverted copy of the originaql sample surface topography and is very stable in the electron beam24 allowing imaging of the surface topography. Note that this "inversion" of the surface topography needs to be accounted for when interpreting the imaging.

Figure 7.3 shows an example of nanocomposite structure when the sample is prepared using the freeze-etching technique. This is a replica of a nanocomposite with CNCs embedded in a thermoplastic starch (TS). The freeze-etching method was used because of hte difficulty to section the starch matrix.[20] The CNCs can be detected in which the contrast is created by platinum metal shadowing. The CNCs appear to be very wide (darker dots in the image), and it is difficult to determine

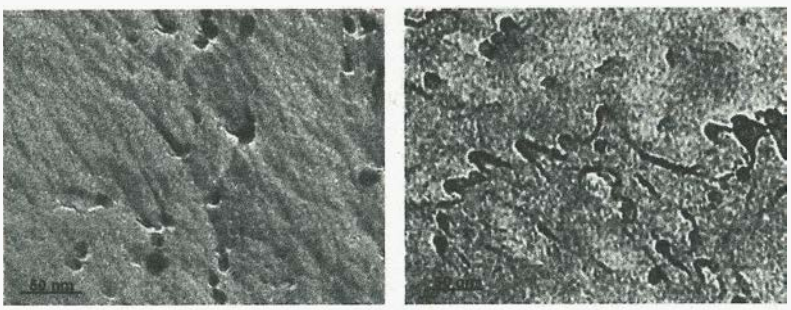

Fig 7.3. TEM images of freeze-etched replicas of TS-CNC nanocomposite (a) parallel view and (b) perpendicular view to the film surface (Adapted from Ref. 20 with permission from Springer)

if the crystals are individual, but they broaden due to metal shadowing or if they are aggregated.

7.3. Characterization of the nanocomposites structure

7.3.1 *Optical microscopy*

OM is not a suitable tool for characterization of nanosize materials such as CN within nanocomposites, but is useful in characterizing the macroscopic composite structure in cases when the matrix is transparent or the sample is very thin. For example, polarized OM can be used to study crystallization behavior of CN composites. Pei *et al.* [25] studied the effect of CNC additions on the crystallization nucleation rate of a PLA polymer. Unmodified CNCs and silylated functionalized CNCs were tested and it was seen that CNC without surface modification aggregated and was not as effective nucleation agent as the silylated CNCs. Figure 7.4 shows the polarized OM images of pure PLA, PLA with 1% CNC, and PLA with 1% silylated crystals in melt at 210°C and how the crystallites nucleate during the cooling, after 0, 5, and 10 min. It is possible to see that the PLA with unmodified CNC has some aggregates compared to the PLA with silylated crystals (0 min).

Kvien and Oksman[26] used polarized OM to study alignment of the CNCs in a PVA matrix using magnetic field. The films were thin and transparent and when viewed in OM, the film was bright at 45° and dark at 0° and 90° between the magnetic field direction and the polarization plane (Fig. 7.5). This OM indicated

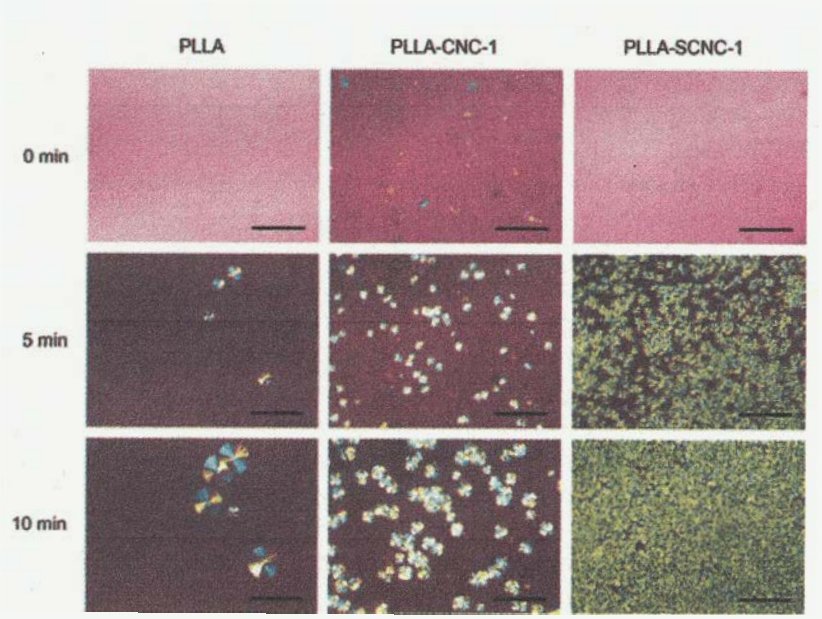

Fig. 7.4. Polarized optical microscope images of PLLA, PLLA-CNC1, and PLLA-SCNC1 after cooling from melt at 210°C showing the ability of CNCs as nucleation agent for PLLA. Scalebar, 200 μm. (The figure is adapted from Ref. 25, with permission from Elsevier.)

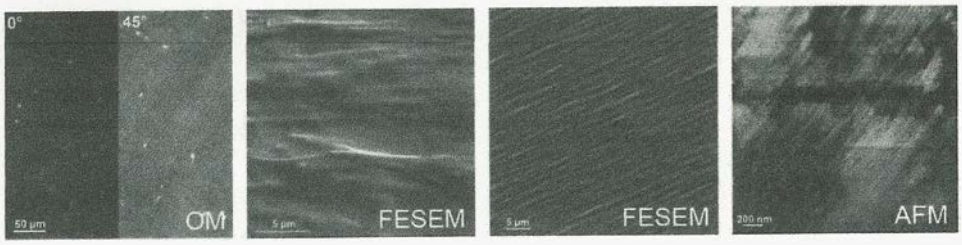

Fig 7.5. Polarized optical microscope images of the nanbocomposite showing reflected light at 45° in polarized light indicating alignment of CNCs the alignment of the CNC is further strengthened by studies with FESEM (fractured and etched surface) and with AFM where highly oriented structures can be seen.

that the CNCs were aligned in the PVA matrix, either parallel or transverse to the field direction. Also, the alignment of the nanocrystals was further studied by FESEM and AFM as seen in Fig. 7.5. The FESEM images of the fractured surface and etched nanocomposites showed a highly oriented structure, similar orientation was seen also in AFM.

7.3.2 *Electron microscopy*

7.3.2.1 *Scanning electron microscopy*

SEM is one of the most used microscopy for materials structure and surface characterization. These microscopes have a resolution between 1 and 5 nm. In addition to the high resolution, they also have a large depth of field, whhich is the reason that the images appear three dimensional. The principle of SEM is that an electron gun generates electrons and accelerates them through lenses which focus the beam with very small spot size. These electrons interact with the specimen to a depth of about 1 µ and generate signals that are used to form the image. The three most important signals are backscattered electrons, secondary electrons, and X-rays. The backscattered electrons are elastically scattered electrons and give compositional contrast depending on the atomic number of the specimen. These electrons have high energy and they come from the depth of the specimen (1 μm or more). Secondary electrons are low energy electrons and come from the top surface of the specimen (a few nm), and are mainly used for topography imaging of the sample. [27]

Cellulose nanocomposites or bionanocomposites contain polymers, where both the matrix and the reinforcing phases are polymeric, which means they are non-conductive and consist of low atomic number elements and, in tipography imaging, mainly used for these materials.

SEM images of two different cellulose nanocomposites are shown in Figs. 7.6 and 7.7. The nanocomposite in Fig. 7.6 shows the fractured surface of PLA nanocomposites with CNC and CNF.[9]

This material was fractured using liquid nitrogen and coated with platinum to avoid charging of the electron beam. It is possible to see that nanocrystals and

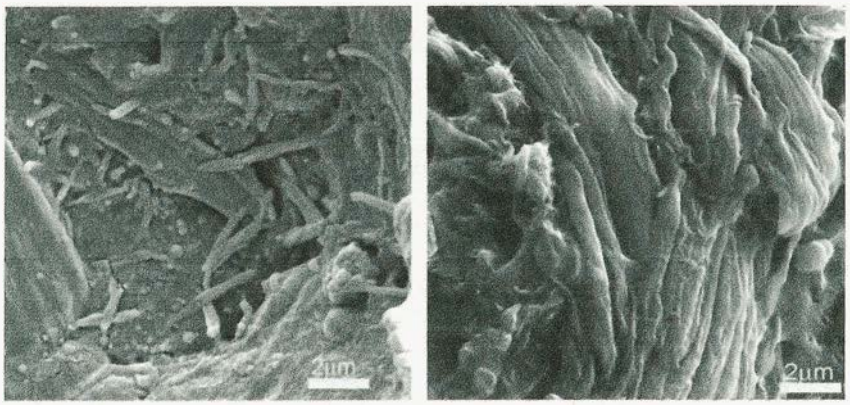

Fig. 7.6. CNCs (left) and cellulose nanofibers (right) in a PLA matrix, It is seen that none of the nanomaterials are well dispersed in the PLA but the nanocrystals are of smaller size and better dispersed and distributed than the nanofibers.

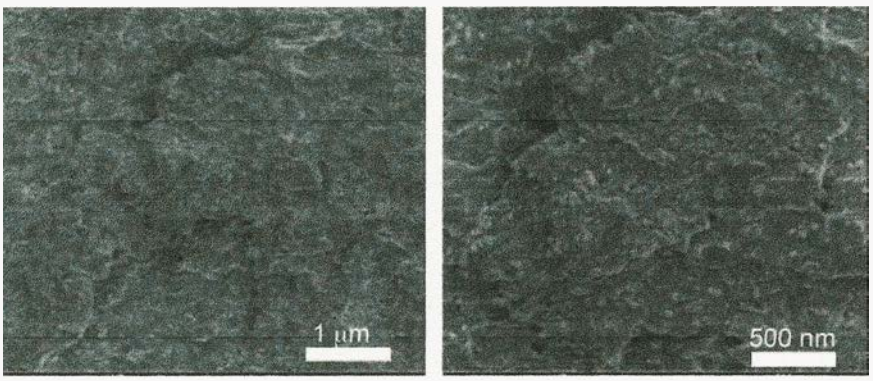

Fig. 7.7. Fractured surface of nanocomposites with CNC (12 wt%) in a CAB matrix. It is seen that CNCs are well distributed and are also dispersed, small dots are seen which are believed to be CNC and no large agglomerate can be seen.

nanofibers are not well dispersed in the PLA matrix, agglomerates in micrometer size are seen.

The second image, Fig. 7.7, shows the fractured structure of nanocomposite with cellulose acetate butyrate (CAB) as matrix and CNC as the reinforcing phase. This sample was not coated, but it was still possible to obtain reasonable resolution using a low voltage of 1 kV in the FESEM. In this case, the CNC was better dispersed in the polymer matrix. There were no visible agglomerates of the crystals in this composite; however, the small spherical particles in the matrix might be cross-sections of small clusters of cellulose crystals in the matrix,[10] In this case, a further investigation of the material in AFM or TEM would give more information of the distribution of CNC in the matrix.

7.3.2.2 *Transmission electron microscopy*

The principle of TEM is that the high energy electrons are transmitted through an ultrathin section of the specimen. The image is formed due to electron scattering when the beam hits the specimen.[28]

The electrons are emitted from an electron gun (filament). Below the electron gun are two or more condenser lenses which demagnify the beam emitted by the gun and control its diameter as it hits the specimen, which is held inside an objective lens just below the condenser lenses. There are two lenses after the objective lens, the intermediate lens and the projector lens. Each produces a real and magnified image, which then produces the image on the fluorescent imaging screen or film. TEM image contrast is due to electron scattering. Bright field (BF) is an imaging mode where an objective aperture is inserted so that the direct unscattered electrons form the image. Regions in the specimen which are thicker or of higher density will scatter more strongly and will appear darker in the image because highly scattered electrons are stopped by the objective aperture. An image field with no specimen in it is bright in BF. In TEM, there are three basic contrast mechanisms, which may contribute to the formation of image:[23,28]

- diffraction contrast,
- mass-thickness contrast, and
- phase contrast.

The cellulose nanocomposites are composed of low atomic number elements and therefore scatter electrons weakly, giving poor contrast in the TEM. For these materials, the mass-thickness contrast mechanism can be exploited by deliberately staining the thin specimen with a heavy metal which highlights specific features of interest. For example, uranyl acetate is one suitable staining agent for CNs to enhance better contrast.[21]

The properties of nanoparticle-reinforced polymer composites are directly affected by the distribution of the nanoparticle phase within the matrix phase. The ability to characterize the nanoparticle distribution along a surface or when embedded within a polymer matrix is critical when relating the resulting composite properties to mechanism of property enhancement.

Transmission electron microscopy is used to analyze the thought thickness of the nanocomposites material and is therefore the most suitable microscopy method, provided the CN distribution and dispersion are of interest.

Bondeson and Oksman[13] studied how the addition of a surfactant affected CNC dispersion and distribution in the PLA matrix. Figure 7.8 shows the FESEM images as well as a TEM image of the CNC composites. The first image is a fractured surface of the PLA nanocomposite where no surfactant was used showing aggregates of CNCs. The second image is also a fractured surface of the nanocomposites with surfactant showing well dispersed and distributed nanocrystals. The last image is TEM of the surfactant sample showing individual CNCs dispersed in the PLA matrix.

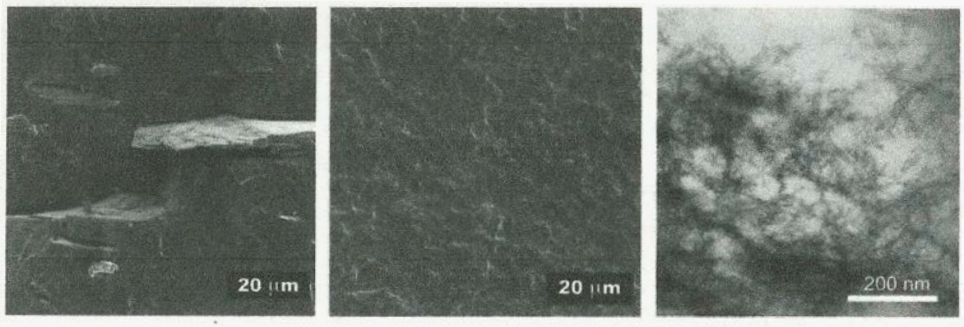

Fig. 7.8. The structure of PLA-CNC nanocomposites viewed with FESEM and TEM. The first image is a composite with poor dispersion and distribution and the second and third images show that the dispersion is affected by a surfactant. The FESEM confirms a better dispersion and distribution of CNC in a PLA and this is further shown by the TEM with individual crystals in PLA.

7.4. Atomic force microscopy

AFM is a scanning probe microscopy technique that can characterize nanometer-scale features of surfaces,[29,30] and has been extensively used in characterizing nanocomposites[31]. A detailed description of the AFM system and technique can be found in Refs. 29, 30, and 31, a brief description is given in Vol. 1.

Topography imaging is usually completed by scanning the AFM probe (typical radius of curvature of 10 nm) over the composite surface while the interaction response between the probe and the sample surface is monitored. Two operating modes can be used (contact and intermittent-contact), and measurements can be completed under different environments (vacuum, vapor, fluid). In the contact mode, the AFM probe tip is scanned across the surface and feedback is used to maintain a constant force between the tip and the sample (see Fig. 7.9). For the intermittent-contact mode (or "tapping" mode), the AFM probe is vibrated near its resonance frequency and feedback is used to maintain a constant force in some aspects of the probe's vibration (such as amplitude). Advantages of intermittent-contact mode are

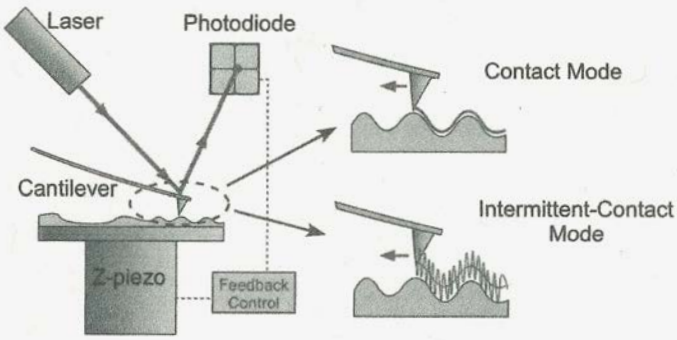

Fig. 7.9. Schematic of AFM setup and the representative configurations of the AFM cantilever/tip and surface for the different imaging modes: contact and intermittent-contact.

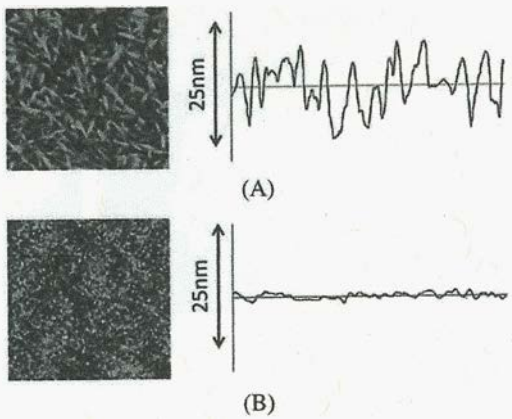

Fig. 7.10. Topography images (3 by 3 μ scans) and roughness profiles (1 μ trace) measured by AFM intermittent-contact mode imaging of cellulose films on silica: (A) CNC film and (B) Langmuir-Schaefer cellulose films (Adapted with permission from Ref. 34. Copyright (2009) American Chemical Society.)

that it has lower lateral forces compared to contact mode and offers the possibility to acquire additional contrast channels such as a phase image.

AFM topography imaging of cellulose nanocomposites has been used to characterize the surface roughness.[32-34] The sub-nanometer quantitative height resolution and qualitative nanometer lateral resolution (depending on tip radius) have allowed for comparative studies on cellulose nanocomposite processing on the resulting surface roughness/finish[32,34] (see Fig. 7.10).

In the intermitted-contact mode, and when feedback is maintained on the amplitude of the probe vibration, information about nanoparticle distribution within polymer matrix composites can be obtained using phase imagining. Phase imaging refers to recording the phase lag (i.e., the "delay") of the cantilever oscillation relative to the signal sent to the cantilever's piezo driver. The phase lag is sensitive to variations in material properties (e.g., adhesion, viscoelasticity, etc.), and thus can create contrast between the different material components within nanocomposites. Additionally, phase imaging highlights edges and is not affected by large-scale height differences, providing clearer observation of fine features, such as grain edges. These characteristics of phase imaging make this technique useful for investigating nanoparticle distribution within polymer composites, which has been completed for various CN-polymer composites15,16,35 (see Fig. 7.11). Since AFM is a surface measurement technique, to characterize the nanoparticle distribution through the composite thickness, it is necessary to image multiple sections through the thickness of the composite.

7.4.1 *AFM — surface chemistry*

AFM techniques have been used to investigate surface chemistry of nanocomposites. The most common technique for these studies is the use of AFM force

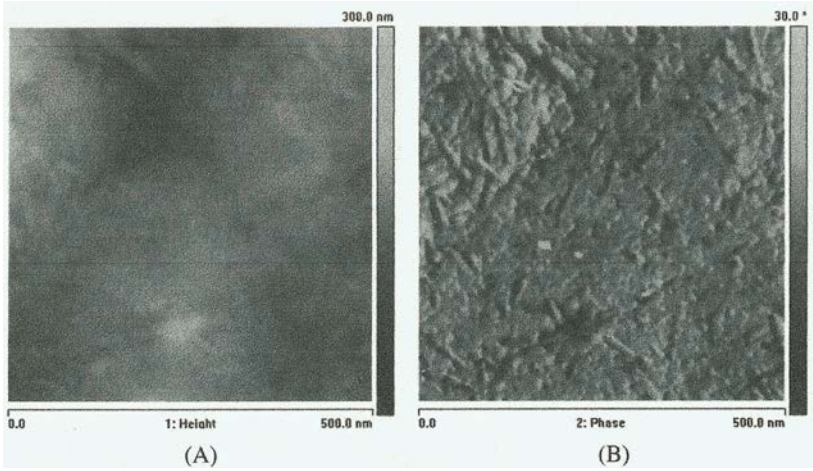

Fig. 7.11. AFM images of 5 wt% CNC-PHBV (poly(3-hdroxybuterate-co-3-hydroxyvalerate)) nanocomposite: (A) topography and (B) phase. In the phase image, the darker colored rod-like CNC particles have increased contrast from the matrix polymer, allowing greater discrimination of the CNC particles from the polymer matrix as compared to that in the topography image (Reprinted from Ref. 35, Copyright (2020) with permission from Elsevier.)

spectroscopy.[36] A detailed description of this technique can be found in Refs. 4, 37, (38, and 39. A brief description is given here. One method of monitoring the interaction between AFM probe tip and that of the sample surface is measuring force–distance (F–D) curves, which summarize the vertical force acting on the AFM tip as it approaches and withdraws from the sample surface (i.e., the distance between the tip and the surface, D).

An idealized F–D plot is given in Fig. 7.12 which shows five general zones: (1) approach, (2) jump-to-contact, (3) indentation, (4) jump-off-contact, and (5) withdrawal. During a typical test, the AFM tip is initially far away from the sample surface that there is minimal interaction (i.e., no force acting on the tip). Jump-to-contact occurs once the tip moves sufficiently close to the surface where the tip–surface attractive force gradient is greater than the cantilever stiffness. Additional applied forces result in the AFM tip indenting into the sample surface, which can be used to extract mechanical properties of the surface. Jump-off-contact happens during the withdrawal, giving information about the adhesive forces (hydrogen, van der Waals, Coulomb, etc.). After this, the tip-sample distance is sufficiently far that no force acts on the tip. The discontinuity of the jump-off-contact can be used to define the force of adhesion (F_{ad}), which can be used to assess the tip-surface interaction.

A single F–D plot provides adhesion/chemical information at the given contact point, whereas to map the adhesion/chemical information for a given area on the surface, multiple F–D plots are needed. Measurements can be completed in vacuum, vapor, or fluids. When testing within vapor, in particular, in ambient conditions with moisture, meniscus formation at the tip-sample contact may occur and the resulting capillary force will contribute to the force of adhesion. By adjusting the chemistry

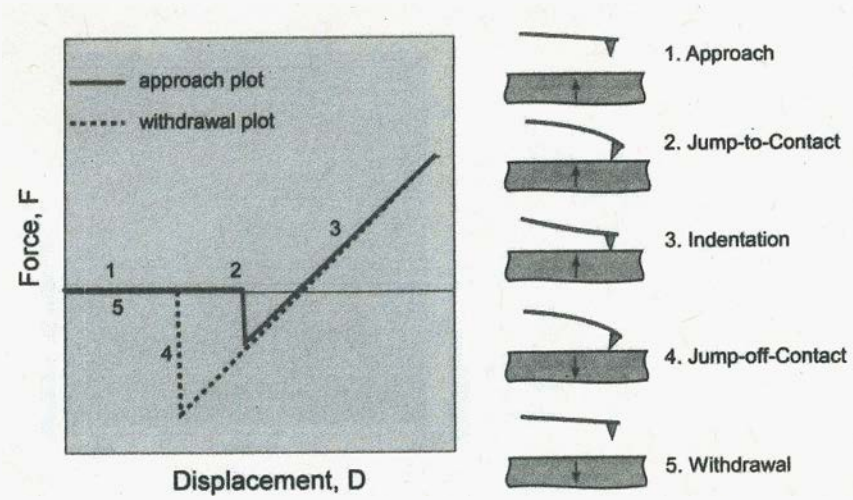

Fig. 7.12. Idealized AFM force-displacement (F-D) plot of AFM tip showing the five stages: (1) approaching, (2) Jump-to-contact, (3) indentation, (4) jump-off-contact, and (5) withdrawing from a surface.

on the AFM tip and the measurement, fluid-specific chemical interactions with a given surface can be investigated.[37,38]

7.5. Cellulose nanoparticle orientation

The mechanical properties of crystalline cellulose (and thus CNCs) are expected to be anisotropic because of the parallel alignment of the cellulose chains along the length of the cellulose crystal. Properties along the crystal length (elastic modulus, E =~145 GPa and ultimate tensile strength, σf = 7.5 GPa) are higher than in perpendicular directions (E = 3 - 50 GPA).[40] Owing to the high axial properties and particle aspect ratio of CNCs, preferentially aligning the particles within a composite to increase properties in the aligned direction has been investigated. Several methods have been used to induce CNC alignment within composites: magnetic fields,[26,41] electric fields,[42,43] mechanical shearing of CNC suspensions,[44,45] combined field and mechanical shearing,[46] drawing of as-cast BC films[47] and cellulose-cellulose composites,[48] and the wet-spinning of CNC composite fibers.[49] Because of the strong influence of CNC orientation on composite properties, this is an important parameter to characterize.

7.5.1 *Wide-angle X-ray diffraction*

The alignment of the CNC within the composites can be characterized via WAXD,[42,44,47-50] in which differences in diffracted X-ray intensities for a given diffraction plane within the cellulose crystal structure are measured as a function of orientation within the composite sample geometry. WAXD measures the diffracting X-rays of a given sample as a function of the diffraction angle (2θ) with

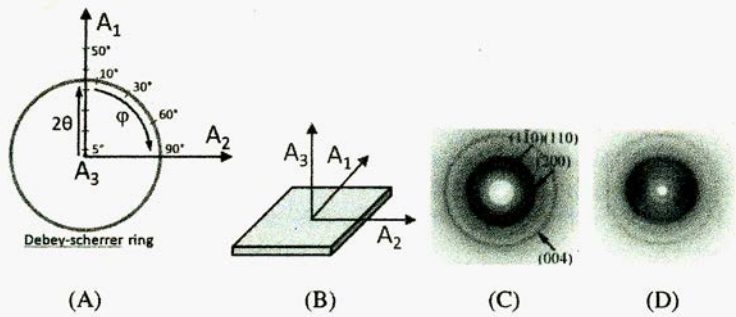

Fig. 7.13. 2D WAXD diffractograms: (A) schematic diffractogram showing *Debye*–Scherrerring, θ, and φ. (B) WAXD can be measured from different composite axis giving additional information on CNC alignment within the composite. (C and D) are diffractograms of a CNC composite,[49] for (C) random CNC alignment showing uniform ring intensity, $I(\varphi)$, and (D) high CNC alignment showing variation in $I(\varphi)$ within a given ring. (Adapted with permission from Ref. 49. Copyright (2011) American Chemical Society.)

respect to the direction of the primary X-ray beam (e.g., monochromatic X-ray, γ = 0.1541 nm, from CuKα radiation generated at a given accelerating voltage and current). Diffracting X-rays occur only at specific conditions based upon the internal crystalline structure of the solid. For cellulose I, diffraction peaks are at 28 of ~14.5°, ~16.6°, ~20.4°, ~22.7°, and ~34.4°, corresponding to the miller indices of the crystallographic planes for Iβ $(1\bar{1}0)$, (110), (102), (200), (004), or Iα (100), (010), $(\bar{1}\bar{1}0)$, (110), and $(\bar{1}\bar{2}3$ & $\bar{1}\bar{1}4)$, respectively.[51,52] Peaks assignments use the Iα and Iβ unit cells of Sugiyama *et al.* in Ref. 53.

The degree of CNC alignment within a composite can be measured from two-dimensional (2D) WAXD diffraction patterns that give diffraction intensities for both 2θ (typically 5–50'), and the azimuthal angle, φ, which is the 360° rotation about one of the axis of the composite sample. The resulting 2D diffraction patterns consist of *Debye*–Scherrer rings which give the azimuthal intensity distribution for each 2θ diffraction peaks (Fig. 7.13A). Since the resulting diffraction patterns are linked with the composite sample, choosing which axis of the composite sample to scan can give additional information regarding the CNC alignment within the composite.[49] Typically for CNC composite films or plates, diffraction patterns are measured in the A_3 direction (see Fig. 7.13B), and for composites with CNC alignment, attempts are made to arrange the composite test sample such that the CNC alignment runs parallel to the A_1 or A_2 axis. For assessing CNC alignment, the (200), (110), or $(1\bar{1}0)$ crystallographic planes (Iβ crystal structure) are measured. The (200) is used to assess the orientation of the CNC fiber axis, whereas the (110) and $(1\bar{1}0)$ can be used to assess the rotation about the CNC fiber axis. The integrated intensity for a given Debye–Scherrer ring is used to calculate the orientation factor:

$$\{\cos^2\varphi\} = \frac{\int_0^{\pi/2} I(\varphi)\cos^2\varphi\sin\varphi d\varphi}{\int_0^{\pi/2} I(\varphi)\sin\varphi d\varphi}, \tag{7.1}$$

where $I(\varphi)$ is the diffracted intensity as a function of azimuthal angle. The more commonly used Herman's order parameter, S, is calculated using the equation

$$S = \frac{1}{2}(3\{\cos^2\varphi\} - 1), \tag{7.2}$$

in which, $S = 0$, for random CN alignment and $S = 1$ for complete CN alignment.

7.5.2 *Atomic force microscopy*

AFM imaging (topography, phase imaging, etc.) has been used to characterize the CNC alignment within nanocomposites[26,33,41,45] in which the degree of CNC alignment can be qualitatively described using various image analysis methods.[45] Typically, the raw AFM image undergoes some post-processing to highlight individual particles and some feature is used to identify the long axis of the CNC. The angle of the long axis of the CNC with respect to a given axis (e.g., sample geometry, or the direction of mechanism that caused CNC alignment) is measured. A histogram is produced that summarizes the percent of CNCs for a given angle from 0 to 90°. Note that such techniques describe a 2D CNC alignment, assuming that all the CNCs lie parallel to the imaging plane of the AFM. To account for this additional degree of freedom in the CNC orientation, a method for characterizing the three-dimensional alignment of short fiber composites using the geometry of the elliptical cross-section shape on a polished surface may be applicable to CNC composites, and for a description of this methodology, the reader can refer to Ref. 54.

7.6. Conclusions

This chapter summarizes several of the more prevalent methods used to date to characterize cellulose nanocomposites (OM, SEM, FESEM, TEM, AFM), and the CNC orientation within the polymer matrix (WAXD, TEM, AFM). For several of these characterization methods, the small size and low atomic number result in some unique challenges for quantitative measurements and require special attention as briefly described. Progress is being made for improved characterization of cellulose nanocomposites, and with this, our understanding of these materials is also growing.

References

1. S.S. Ray and M. Okamoto, Polymer/layered silicate nanocomposites: a review from preparation to processing. *Prog. Polym. Sci.* **28** (2003) 1539–1641.
2. D. Bondeson, A.P. Mathew and K. Oksman, Optimization of the isolation of nanocrystals from microcrystalline cellulose by acid hydrolysis. *Cellulose* **13** (2006) 171–180.
3. G. Gong, A.P. Mathew and K. Oksman, Strong aqueous gels of cellulose nanofibers and nanowhiskers isolated from softwood flour, *TAPPI J.* 10 (2011).
4. R.R. Lahiji, X. Xu, R. Reifenberger, A. Raman, A. Rudie and R. J. Moon, Atomic force microscopy characterization of cellulose nanocrystals, *Langmuir* **26** (2010) 4480-4488.
5. T. Saito, S. Kimura, Y. Nishiyama and A. Isogai, Cellulose nanofibers prepared by TEMPO-mediated oxidation of native cellulose, *Biomacromol.* **8** (2007) 2485–2491.

6. M.A.S. Azizi Samir, F. Alloin and A. Dufresne, Review of recent research into cellulosic whiskers, their properties and their application in nanocomposite fields. *Biomacromol.* **6** (2005) 612-626.
7. B.S. Tanem, I. Kvien and K. Oksman, *Morphology of cellulose and its nanocomposites.* In *Cellulose nanocomposites: processing, characterization and properties,* K. Oksman and M. Sain (Eds.) Oxford Press (2006), ACS Symposium Series, Vol. 938.
8. E. Trovatti, L. Oliveira, C.S.R. Freire, A.J.D. Silvestre, C. Pascoal Neto, J.J.C. Cruz Pinto and A. Gandini, Novel bacterial cellulose–acrylic resin nanocomposites, *Compos. Sci. Technol.* **70** (2010) 1148–1153.
9. A.P. Mathew, A. Chacraborty, K. Oksman and M. Sain, The Structure and mechanical properties of cellulose nanocomposites prepared by twin screw extrusion. In *Cellulose nanocomposites: processing, characterization and properties.* K. Oksman and M. Sain, (Eds.) Oxford Press (2006), ACS Symposium Series, Vol 938.
10. G. Siqueira, A.P. Mathew and K. Oksman, Processing of cellulose nanowhiskers/ cellulose acetate butyrate nanocomposites using sol-gel process to facilitate dispersion, *Comp. Sci. Technol.* **71** (2011), 1886–1892.
11. A.J. Svagan, P. Jensen, S.V. Dvinskikh, I. Furo and L.A. Berglund, Towards tailored hierarchical structures in cellulose nanocomposites biofoams prepared by freezing/freeze-drying, *J. Mater. Chem.* **20** (2010) 6646–6654.
12. L. Petersson, I. Kvien and K. Oksman, Structure and thermal properties of polylactic acid/cellulose whiskers nanocomposites, *Compos. Sci. Technol.* **67** (2007) 2535–2544.
13. D. Bondeson and K. Oksman, Dispersion and characteristics of surfactant modified cellulose whiskers nanocomposites, *Comp. Interf.* **14** (2007) 617–630.
14. I. Kvien, B.S. Tanem and K. Oksman, Characterization of cellulose whiskers and its nanocomposites by atomic force and electron microscopy, *Biomacromol.* **6** (2005) 3160–3165.
15. L. Goetz, A. Mathew, K. Oksman, P. Gatehnolm and A.J. Ragauskas, A novel nanocomposite film prepared from crosslinked cellulosic whiskers, *Carbohydr. Polym.* **75** (2009) 85–89.
16. J.E. Ayuk, A.P. Mathew and K. Oksman, The effect of plasticizer and cellulose nanowhisker content on the dispersion and properties of cellulose acetate butyrate nanocomposites, *J. Appl. Polym. Sci.* **114** (2009) 2723–2730.
17. A.P. Mathew, M-P.G. Laborie and K. Oksman, Cross-linked chitosan/chitin crystal nanocomposites with improved permeation selectivity and Ph stability, *Biomacromol.* **10** (2009) 1627–1632.
18. K. Oksman, A.P. Mathew, D. Bondeson and I. Kvien, Manufacturing process of polylactic acid (PLA) – cellulose whiskers nanocomposites, *Compos. Sci. Technol.* **66** (2006) 2776–2784.
19. D. Wang, J. Yu, J. Zhang, J. He and J. Zhang, Transparent bionanocomposites with improved properties from poly (propylene carbonate) (PPC) and cellulose nanowhiskers (CNWs), *Compos. Sci. Technol.* **85** (2013) 83–89.
20. I. Kvien, J. Sugiyama, M. Vortrubec and K. Oksman, Characterization of starch based nanocomposites, *J. Mater. Sci.* **42** (2007) 8163-8171.
21. I. Kvien and K. Oksman, Microscopic examination of cellulose whiskers and their nanocomposites. In *Characterization of lignocellulosic materials,* T.Q. Hu (Ed.) Oxford, UK: Blackwell Publishing (2008), Ch. 20, p.342–356.
22. NIKON Microscopy U, the source for microscopy education. Available at: http://www.microscopyu.com/articles/formulas/formulasresolution.html
23. L.C. Sawyer and D.T. Grubb, *Polymer microscopy,* 1st edn. London: Chapman and Hall (1987).
24. J.H.M. Willison and A. J. Rowe. Replica, shadowing and freeze-etching techniques. In *Practical methods in electron microscopy,* M. Audrey Glauert (Ed.) Elsevier/North-Holland: Biomedical Press (1980).

25. A. Pei, Q. Zhou and L.A. Berglund, Functionalized cellulose nanocrystals as biobased nucleation agents in poly (L-lactide) (PLLA) – crystallization and mechanical property effects, *Compos. Sci. Tech.* **70** (2010) 815-821.
26. I. Kvien and K. Oksman, Orientation of cellulose nanowhiskers in polyvinyl alcohol, *Appl. Phys. A.* **87** (2007) 641-643.
27. J. Goldstein, D. Newbury, D. Joy, D. Lyman, P. Echlin, E. Lifshin, L. Sawyer and J. Michael, *Scanning electron microscopy and X-ray microanalysis,* 3rd edn. New York: Kluwer Academic/Plenum Publishers (2003).
28. P.J. Goodhew, J. Humphreys and R. Beanland, *Electron microscopy and analysis,* London: Taylor & Francis (2001).
29. P.C. Braga and D. Ricci, *Atomic force microscopy: biomedical methods and applications,* Springer **242** (2004).
30. P. Eaton and P. West, *Atomic force microscopy,* Cary, NC, USA: Oxford University Press, (2010).
31. S. Bandyopadhyay, S.K. Samudrala, A.K. Bhowmick and S.K. Gupta. Applications of atomic force microscope (AFM) in the field of nanomaterials and nanocomposites. In *Functional nanostructures: processing, characterization, and applications,* S. Seal, (Ed,) Springer, 2007. pp. 504-568.
32. E.E. Brown and M-P.G. Laborie, Bioengineering bacterial cellulose/poly(ethylene oxide) nanocomposites, *Biomacromol.* **8** (2007) 3074-3081.
33. B. Jean, F. Dubreuil, L. Heux and F. Cousin, Structural details of cellulose nanocrystals/polyelectrolytes multilayers probed by neutron reflectivity and AFM, *Langmuir* **24** (2008) 3452-3458.
34. C. Aulin, S. Ahola, P. Josefsson, T. Nishino, Y. Hirose, M. Osterberg and L. Wagberg, Nanoscale cellulose films with different crystallinities and mesostructures-their surface properties and interaction with water, *Langmuir* **25** (2009) 7675-7685.
35. E. Ten, J. Turtel, D. Bahr, L. Jiang and M. Wolcott, Thermal and mechanical properties of poly(3-hydroxybutyrate-co-3-hydroxyvalerate)/cellulose nanowhiskers composites, *Polymer* **51** (2010) 2652-2660.
36. H. Butt, B. Cappella and M. Kappl, Force measurements with the atomic force microscope: technique, interpretation and applications, *Surf. Sci. Rep.* **59** (2005) 1-152.
37. X. Zhang and R. Young, Adhesion properties of cellulose films, *Mater. Res. Soc. Symp. Proc.* **586** (2000) 157-162.
38. J.C. Bastidas, R. Venditti, J. Pawlak, R. Gilbert, S. Zauscher and J.F. Kadla, Chemical force microscopy of cellulosic fibers, *Carbohydr. Polym.* **62** (2005) 369-378.
39. R.R. Lahiji, Y. Boluk and M. McDermott, Adhesive surface interactions of cellulose nanocrystals from different sources, *J. Mater Sci.* **47** (2012) 3961-3970.
40. R.J. Moon, A. Martini, J. Nairn, J. Simonsen and J. Youngblood, Cellulose nanomaterials review: structure, properties and nanocomposites, *Chem. Soc. Rev.* **40** (2011) 3941-3994.
41. E.D. Cranston and D.G. Gray, Formation of cellulose-based electrostatic layer-by-layer films in a magnetic field, *Sci. Technol. Ad. Mater.* **7** (2006) 319-321.
42. W. Gindl, G. Emsenhuber, G. Maier and J. Keckes, Cellulose in never-dried gel oriented by an AC electric field, *Biomacromol.* **10** (2009) 1315-1318.
43. Y. Habibi, T. Heim and R. Douillard, AC electric field-assisted assembly and alignment of cellulose nanocrystals, *J. Polym.* Sci. *Part B* **46** (2008) 1430-1436.
44. Y. Nishiyama, K. Shigenori, W. Masahisa and O. Takeshi, Cellulose microcrystal film of high uniaxial orientation, *Macromol.* **30** (1997) 6395-6397.
45. I. Hoeger, O.J. Rojas, K. Efimenko, O.D. Velev and S.S. Kelley, Ultrathin film coatings of aligned cellulose nanocrystals from a convective-shear assembly system and their surface mechanical properties, *Soft Matter* **7** (2011) 1957-1967.

46. L. Csoka, I.C Hoeger, P. Peralta, I. Peszlen and O.J. Rojas, Dielectrolphoresis of cellulose nanocrystals and alignment in ultrathin films by electric field-assisted shear assembly, *J. Coll. Int. Sci.* **363** (2011) 206-212.
47. A. Bohn, H.P. Fink, J. Ganster and M. Pinnow, X-ray texture investigations of bacterial cellulose, *Macromolecular Chem. Phys.* **201** (2000) 1913–1921.
48. W. Gindl and J. Keckes, Drawing of self-reinforced cellulose films, *J. Appl. Polym. Sci.* **103** (2007) 2703-2708.
49. S. Iwamoto, A. Isogai and T. Iwata, Structure and mechanical properties of wet-spun fibers made from natural cellulose nanofibers, *Biomacromol.* **12** (2011) 831-836.
50. H. Sehaqui, N.E. Mushi, S. Morimune, M. Slakjkova, T. Nishino and L.A. Berglund, Cellulose nanofibers orientation in nanopaper and nanocomposites by cold drawing, *ACS Appl. Mater. Interf.* **4** (2012) 1043-1049.
51. M. Wada, J. Sugipma and T. Okano, Native cellulose on the basis of two crystalline phase (Ia/Ib) system, *J. Appl. Poly. Sci.* **49** (1993) 1491-1496.
52. A. Thygesen, J. Oddershede, H. Lihot, A.B. Thomsen and K. Stahl, On the determination of crystallinity and cellulose content in plant fibres, Cellulose **12** (2005) 563-576.
53. S. Sugiyama, R. Vuong and H. Chanzy, Electron diffraction study on the two crystalline phases occurring in native cellulose from an algal cell wall, *Macromol.* **14** (1991) 4168-4175.
54. Y.H. Lee, S.W. Lee, J.R. Youn, K. Chung and T.J. Kang, Characterization of fiber orientation in short fiber reinforced composites with an image processing technique, *Mat. Res. Innovat.* **6** (2002) 65–72.

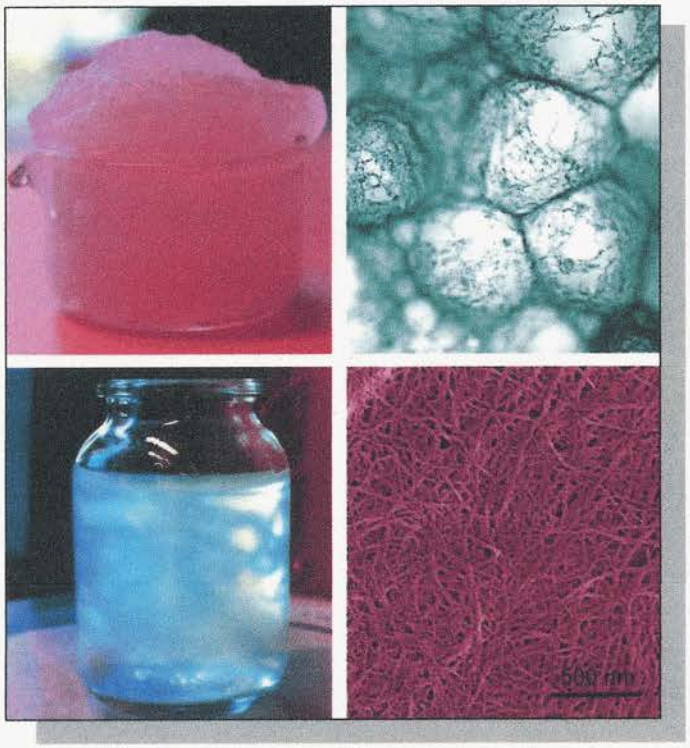

MATERIALS AND ENERGY – Vol. 5

HANDBOOK OF GREEN MATERIALS

❷ Bionanocomposites: processing, characterization and properties

Editors

Kristiina Oksman • Aji P Mathew
Alexander Bismarck • Orlando Rojas
Mohini Sain

World Scientific

Published by

World Scientific Publishing Co. Pte. Ltd.
5 Toh Tuck Link, Singapore 596224
USA office: 27 Warren Street, Suite 401-402, Hackensack, NJ 07601
UK office: 57 Shelton Street, Covent Garden, London WC2H 9HE

British Library Cataloguing-in-Publication Data
A catalogue record for this book is available from the British Library.

World Scientific Series in Materials and Energy
HANDBOOK OF GREEN MATERIALS
Processing Technologies, Properties and Applications
(In 4 Volumes)

Copyright © 2014 by World Scientific Publishing Co. Pte. Ltd.

All rights reserved. This book, or parts thereof, may not be reproduced in any form or by any means, electronic or mechanical, including photocopying, recording or any information storage and retrieval system now known or to be invented, without written permission from the Publisher.

For photocopying of material in this volume, please pay a copying fee through the Copyright Clearance Center, Inc., 222 Rosewood Drive, Danvers, MA 01923, USA. In this case permission to photocopy is not required from the publisher.

ISBN 978-981-4566-45-2 (Set)
ISBN 978-981-4566-48-3 (Vol. 1)
ISBN 978-981-4566-49-0 (Vol. 2)
ISBN 978-981-4566-50-6 (Vol. 3)
ISBN 978-981-4566-51-3 (Vol. 4)

Typeset by Stallion Press
Email: enquiries@stallionpress.com

Printed by FuIsland Offset Printing (S) Pte Ltd Singapore